Adsorption of water, methanol and their mixtures in slit graphite pores

Paulina Pršlja,[1, a)] Enrique Lomba,[1] Paula Gómez-Álvarez,[1, b)] Tomaz Urbič,[2] and Eva G. Noya[1]

[1)] *Institute of Physical Chemistry "Rocasolano", Serrano 119, E-28006 Madrid, Spain.*

[2)] *Faculty of Chemistry and Chemical technology, University of Ljubljana,Ljubljana, Slovenia.*

(Dated: 11 December 2018)

The behavior of water, methanol and water-methanol mixtures confined in narrow slit graphite pores as a function of pore size was investigated by Monte Carlo, hybrid Monte Carlo and Molecular Dynamics simulations. Interactions were described using TIP4P/2005 for water, OPLS/2016 for methanol and cross interactions fitted to excess water/methanol properties over the whole range of concentrations, which provide a rather accurate description of water-methanol mixtures. As expected for hydrophobic pores, whereas pure methanol is adsorbed already from the gas phase, pure water only enters the pore at pressures well beyond bulk saturation for all pore sizes considered. When adsorbed from a mixture, however, water adsorbs at much lower pressures due to the formation of hydrogen bonds with previously adsorbed methanol molecules. For all studied compositions and pore sizes, methanol adsorbs preferentially over water at liquid-vapor equilibrium conditions. In pure components, both water and methanol are microscopically structured in layers, the number of layers increasing with pore size. This is also the case in adsorbed mixtures, in which methanol has a higher affinity for the walls. This becomes more evident as the pore widens. Diffusion of pure water is higher than that of pure methanol for all pore sizes due to the larger size of the methyl group. In mixtures, both components present similar diffusivities at all pore sizes, which is explained in terms of the coupling of molecular movements due to strong hydrogen bonding between methanol and water molecules. This is particularly evident in very narrow pores, in which pure methanol diffusion is completely impeded on the time scale of our simulations, but the presence of a small amount of water molecules facilitates alcohol diffusion following a single-file mechanism. Additionally, our results indicate that pure water diffusivities display a non-monotonous dependence of pore size, due to effects of confinement (proximity to a fluid-solid-fluid transition induced by confinement as reported in previous work) and the dynamic anomalies of water.

Keywords: adsorption, slit pores, water/methanol mixtures, computer simulation

---

[a)]Now at Institute of Chemical Research of Catalonia (ICIQ), Avinguda dels Països Catalans, 16, E-43007 Tarragona, Spain.

[b)]Now at Laboratorio de Simulación Molecular y Química Computacional, CIQSO, and Departamento de Ciencias Integradas, Universidad de Huelva, E-21007 Huelva, Spain.

I. INTRODUCTION

Adsorption of water/alcohol mixtures on porous materials is an important topic, both from an applied and a fundamental point of view. Understanding confinement effects on water/alcohol solutions can have impact in many different fields, ranging from the bio-fuel industry[1] to biological systems. Confined fluids often exhibit a completely different behavior from that of the bulk, and the study of simple pore geometries, such as cylinders or slit pores can further our understanding of the new features induced by confinement. Moreover, these simple geometries are often useful as idealized representations of otherwise complex porous materials such as one-dimensional channel zeolites (cylindrical pores) or clays and graphitized porous carbons (slit pores).

Since water is ubiquitous in natural and industrial processes, a large number of experimental and simulation works have addressed its behavior under confinement, either into cylindrical pores (such as nanotubes), or in slit pores (with hydrophobic, hydrophilic or mixed pore walls)[2–12]. In the latter instance, it has been shown that water is structured in layers, which at sufficiently high pressures can crystallize into solids with structures very different from those found in the bulk system. For example, recent experiments indicate that water confined between graphite walls with a separation of about 1 nm might form a square ice structure that is not found in bulk[6]. Simulation studies, on the other hand, predict different structures depending on the water model used, some models confirming the experimental square ice lattice[13,14]. Many of the studies of confined water focus on the effects of confinement on the anomalous behavior of water. Very specially, confined systems were used to probe the potential existence of a second critical point[4] which has been assumed to be the source of the anomalous behavior of water. Since confinement in hydrophobic pores tends to preclude crystallization[15], the region where a second critical point might occur becomes accessible. In this connection, recently Nomura and coworkers[16] have also provided computer simulation evidence of the coexistence of two liquid phases of water confined in 1.25 nm diameter nanotubes. Simulations have also indicated that the thermodynamic and dynamic behavior of confined water in 1.1nm wide slit pores should be very similar to that of bulk water at temperatures 40 K higher[4]. Anomalous behavior under hydrophobic confinement should be expected then at temperatures lower than in the bulk[4].

On the other hand, studies addressing the adsorption of alcohol and water/alcohol mix-

tures in simple geometries are comparatively more scarce, although the topic has gained some attention during the last few years[17–26]. Experiments of adsorption of pure methanol were carried out mainly in carbon black, activated carbon or in crystalline carbon pores with hexagonal shape[27–29]. The adsorption in a simple slit geometry was investigated in a few simulation studies, that showed that adsorption occurs below bulk saturation pressure for pores narrower than 2nm and that methanol forms chains for narrow pores, which are perturbed as pore size increases[24–26]. Regarding adsorption of water/alcohol mixtures, which are completely miscible in bulk, recent experiments indicate that demixing might take place when the solution is confined between hydrophilic (mica) and hydrophobic (graphite) plates[17–19]. According to these experiments, alcohol molecules aggregate at the graphite/water interface forming two-dimensional islands that sit on top of a monolayer of water above the mica surface. Both the size and shape of the alcohol islands depend on the length of the alcohol chain. Diffusion rates are also affected by confinement, to the point that they can be up to six orders of magnitude lower than in bulk[17–19]. Molecular dynamics simulations of water/alcohol mixtures confined between two graphene layers[21] show that, similarly to water, molecules in these solutions are also structured in layers under parallel hydrophobic confinement. These simulations predict that as pore size increases a gradient of alcohol concentration is induced, with alcohol molecules arranged preferentially in the vicinity of the pore walls. Alcohol and water diffuse together due to alcohol-water association, a fact that has also been reported in the bulk system[30,31]. More recently, a comparative study of the adsorption of ethanol/water mixtures in graphene and hexagonal boron nitride (hBN) slit pores has shown that alcohol selectivity is maximum in hBN pores and at intermediate pore size (around 0.9 nm wide pores)[23]. In all these studies configurations of the confined fluid were generated using a setup in which the slit pore is in contact with two bulk reservoirs, with a pressure gradient applied until a steady state fluid flow is reached inside the pore. Then reservoirs are removed and the pore and the confined molecules are periodically replicated along the pore main axis. Finally, the fluid is re-equilibrated and the simulations continued in the canonical or isothermal-isobaric ensembles.

In this work we present a simulation study of the adsorption of water, methanol and their mixtures in narrow slit graphite pores in which the adsorbed fluid is in equilibrium with an infinite reservoir at moderate pressures. Here water, methanol and their cross interactions are described using the the force-fields that currently yield the most faithful description

of the bulk systems, namely, TIP4P/2005[32] for water, and OPLS/2016[33] for methanol, in combination with cross-interactions fitted to reproduce the experimental excess properties of the mixtures over the whole composition range[34]. In contrast with most previous simulation studies of adsorption into pores of simple geometry (in particular those for the mixtures), fluid adsorption has been studied here using Grand Canonical ensemble simulations. For the pure substances the room temperature adsorption isotherms have been here calculated to estimate the adsorption onset pressure. Chemical potentials (μ, needed in the Grand Canonical ensemble) were connected to pressures (p, the experimentally accessible quantity in adsorption experiments) via an equation of state (EoS) determined by means of extensive simulations in the canonical ensemble. For the mixtures, adsorption simulations were performed at experimental liquid-vapor equilibrium conditions, i.e. the confined fluid mixture is in equilibrium with a vapor reservoir whose composition (chemical potential of each component) is the one that would be in equilibrium with a liquid solution with a predefined composition. Using Grand Canonical Monte Carlo simulations (GCMC), hybrid GCMC-Molecular Dynamics (MD) and canonical ensemble (NVT) MD simulations we have then studied here the structure and dynamics of the confined pure water and methanol and their mixtures. We have analyzed their behavior as a function of the pore size and the composition of the liquid solution in equilibrium with the adsorbed fluid, in order to find the concentration conditions and pore size that would render the optimal selectivity in a potential alcohol/water separation process, either based on equilibrium adsorption or in diffusion.

II. MODELS AND SIMULATION METHOD

A. Model potentials

In this work water and methanol were described using TIP4P/2005[35] and OPLS/2016[33] rigid non-polarizable models. TIP4P/2005 is a four site water model that carries a Lennard-Jones (LJ) center on the oxygen, positive charges on the hydrogen atoms and a negative charge at the M-site that is located along the bisector of the H-O-H angle[35]. OPLS/2016 has three interaction sites, two LJ centers, at the oxygen and methyl group, and point charges at the oxygen, hydrogen and methyl group sites[33]. Both TIP4P/2005 and OPLS/2016 are the rigid non-polarizable models that provide the best overall description of water and

methanol over the whole phase diagram[33,36], including the vapor-liquid equilibrium, which is in both instances used to fit the model potential parameters. Water-methanol cross LJ parameters were taken from Ref. 34, where they were fitted to reproduce the experimental excess volume and enthalpy of water-methanol mixtures throughout the composition range. Note that usual Lorentz-Berthelot or geometric combining rules often give a rather poor description of alcohol-water mixtures[34,37], which stresses the need for a careful choice of appropriate cross interaction parameters. In a previous work, we have seen that the choice of the water model can have a large impact on co-adsorption of water in the adsorption alcohol-water mixtures in hydrophobic pores[38], and we speculate that the same is true for the cross water-alcohol interactions. Thus, it is important to use the best available force-field to describe the interactions in the system. All the parameters for water, methanol and water-methanol interactions are collected in Table I.

The graphite slit pores were modeled by placing two graphite surfaces separated away from each other by a distance (pore width) H. Three different pore sizes were considered, namely H=7 Å, 10 Å and 15 Å. Intralayer carbon-carbon bond length was set to 1.42 Å with a graphite interlayer distance of 3.4 Å[10]. Carbon atoms were frozen during simulations, a common approach that is not expected to affect much the adsorption behavior. Each carbon atom was modeled as a LJ center whose cross interactions with water were taken from the bibliography[10], whereas those of methanol were estimated from the Lorentz-Berthelot combining rules using carbon parameters from alkane-graphite interactions, taken from Ref. 8. Note that we have entirely neglected the presence of quadrupoles on the graphite carbon atoms. When explicitly included in the potential model, these terms account for 30∼40 % of the attractive interaction, as compared with the purely dispersive contributions[39]. Here, as in most previous works we have used plain Lennard-Jones potentials with parameters originally fitted from experimental data, and thus including permanent and induced multipole interactions in an effective fashion. As a matter of fact, our model gives for the water monomer graphite binding energy -7.05 kJ/mol, which compares reasonably well with the value -6.33 kJ/mol, obtained by Weder et al[40] fitting the experimental contact angle of water droplets on graphite surfaces modeling the system with SPC/E water.

Adsorbate-carbon cross interactions are collected in Table II. Each graphite surface contains two atomic graphene layers of area 31.92 Å×34.02 Å. Periodic boundary conditions[41] were applied along the three dimensions of space, so that the simulated system corresponds

TIP4P/2005[32]		OPLS/2016[33]		Water-methanol[34]	
ϵ_{O_W} (K)	93.2	ϵ_{O_M} (K)	97.775	$\epsilon_{O_W-O_M}$ (K)	85.653
σ_{O_W} (Å)	3.1589	σ_{O_M} (Å)	3.1659	$\sigma_{O_W-O_M}$ (Å)	3.1793
q_M (e)	-1.1128	ϵ_{CH_3} (K)	110.45	$\epsilon_{O_W-CH_3}$ (K)	145.215
q_{H_W} (e)	0.556	σ_{CH_3} (Å)	3.6499	$\sigma_{O_W-CH_3}$ (Å)	3.401
		q_{O_M} (e)	-0.6544		
		q_{H_M} (e)	0.4998		
		q_{CH_3} (e)	0.1546		

TABLE I. Model parameters for water-water, methanol-methanol and water-methanol interactions.

Carbon-water[10]		Carbon-methanol[8,33]	
ϵ_{C-O_W} (K)	46.60	ϵ_{C-O_M} (K)	52.32
σ_{C-O_W} (Å)	3.262	σ_{C-O_M} (Å)	3.283
		ϵ_{C-CH_3} (K)	55.611
		σ_{C-CH_3} (Å)	3.525

TABLE II. Cross LJ parameters for carbon-water and carbon-methanol interactions. Carbon-methanol parameters were estimated using Lorentz-Berthelot combining rules, in conjunction with OPLS/2016 methanol and carbon LJ interactions provided in Ref. 8.

to a periodic arrangement of slit pores separated by a distance of 10.2 Å (or roughly 13.5 Å, if we take into account the size of carbon atoms). Note that interactions between neighboring pores do not vanish due to the long range of the electrostatic potential, but in any case are expected to be small.

B. Simulation details

Grand Canonical Monte Carlo, NVT Molecular Dynamics, or hybrid GCMC-MD simulations were used depending on the property of interest employing the LAMMPS[42] package. In the latter instance a series of NVT MD steps is alternated with a series of GCMC particle insertion/deletion and translation/rotational move attempts. Lennard-Jones potential was

truncated at 12 Å, whereas the particle-particle particle-mesh[43] (P^3M) method was used to estimate long range electrostatic interactions. In all the MD simulations time step was set to 1 fs. Temperature was set at 298 K using Nose-Hoover thermostat[44,45] with a damping constant of 0.1 ps. From our previous studies on alcohol/water adsorption into hydrophobic substrates[38] we do not expect significant changes from moderate increases of temperature (up to 30K). An increase in temperature shifts the onset of adsorption isotherms to higher pressures, since a higher kinetic energy overcomes the binding energy of adsorbates at very low loadings. Otherwise, the qualitative adsorption behavior remains unchanged. From an structural point of view, increasing the temperature would tend to break up more easily the less energetic hydrogen bonds between methanol molecules, which would remain linked in three dimensional structures to water molecules, disrupting the tendency of methanol to form linear chains.

In order to compute the EoS ($\mu - p$ relation) of the pure substance, we have first performed hybrid GCMC simulations of bulk water and bulk methanol at different values of chemical potential. Simulations consisted on 20-30 million MD steps, discarding the first 10^6 for equilibration. Every 100 MD steps 100 MC particle exchange attempts plus another 100 displacements/rotations were attempted. Maximum particle displacement and orientational moves were adjusted to obtain a 20-50 % acceptance probability. Using the final configurations of GCMC-MD hybrid simulations, we started MD simulations in the NVT ensemble, in which pressure was estimated by the virial route. Additionally, these simulations provide an assessment on the reliability of our hybrid GCMC-MD results through a thermodynamic consistency check. To that aim the chemical potential at a given pressure estimated from the GCMC-MC simulations is to be compared with that obtained from the thermodynamic integration of the EoS, starting from a different thermodynamic state (see Section III and Refs. 41 and 46).

Next hybrid GCMC-MD simulations were used to estimate the adsorption isotherms of pure water and pure methanol at 298 K in graphite slit pores. Simulations consisted now on $2 \times 10^6 - 3 \times 10^6$ steps discarding 10^6 for equilibration. The EoS obtained with the previous set of simulations were used to relate the chemical potential with the pressure in the reservoir in equilibrium with the confined fluid.

The adsorption of water-methanol mixtures was studied at liquid-vapor equilibrium conditions. In this case we have used plain GCMC simulations, since hybrid GCMC-MD for

molecular mixtures is not currently implemented in LAMMPS. The vapor composition of the reservoir and the corresponding water and methanol chemical potentials needed for the GCMC simulation, were determined assuming that the vapor is in equilibrium with a liquid of known composition, using the experimental vapor-liquid equilibrium data[47]. In particular, chemical potentials were obtained from the mixture compositions in the gas phase in conjunction with ideal gas law. A more elaborate alternative would be the use of the extended isothermal-isobaric Gibbs ensemble with three simulation boxes (confined fluid, vapor, and liquid in equilibrium) as used by Bai et al.[48] to study alcohol/water adsorption in zeolites. Since our models have shown to be accurate for the liquid-vapor equilibrium of both pure substances and the excess thermodynamic properties over whole composition range of the mixture, we are confident that the use of the experimental EoS is justified. Finally, simulations have been performed for three liquid mixture compositions, namely, dilute alcohol ($x^l_{MeOH} = 0.020$), alcohol poor ($x^l_{MeOH} = 0.115$) and alcohol rich ($x^l_{MeOH} = 0.692$). Runs consisted on 5×10^5 MC cycles discarding the first 10^5 for equilibration. A cycle is defined as 50 molecule insertion/deletion attempts plus 50 displacement/rotation attempts of a water molecule together with 50 displacement/rotation attempts of a methanol molecule. In this case, results were averaged over four independent trajectories.

The average density of the adsorbed fluid was estimated using:

$$\rho = \frac{\langle N_{H_2O} + N_{MeOH} \rangle}{L_x L_y L'_z}, \tag{1}$$

where angular brackets denote ensemble average, N_{H_2O} and N_{MeOH} are, respectively, the number of adsorbed water and methanol molecules, L_x, L_y the planar dimensions of the graphite plates and L'_z is the effective pore width. Here it is defined as $L'_z = H - \sigma_{C-O_W}$ to take into account that adsorbed molecules do not have access to the whole pore volume due to the finite size of the adsorbate and adsorbent atoms.

The final configurations of the simulations in the grand canonical ensemble of the adsorption of pure components and the mixtures were then used as the starting configurations of NVT MD simulations. The system was allowed to evolve for 5×10^5-10^6 time steps, discarding 10^5 for equilibration. Density profiles of the adsorbed fluid along the direction perpendicular to the pore walls, and diffusion coefficients were evaluated along these trajectories. The density profiles $\rho(z)$ were calculated using:

$$\rho(z) = \frac{\langle N_i(z + \Delta z) \rangle}{L_x L_y \Delta z} \tag{2}$$

where $\langle N_i(z+\Delta z)\rangle$ is the ensemble average of the number of particles in the slab of fluid between z and $z+\Delta z$. Einstein's relation was used to estimate the diffusion constant D from the mean squared displacement:

$$D = \frac{1}{2d}\lim_{t\to\infty}\frac{d\langle|\mathbf{r}_i(t)-\mathbf{r}_i(t_0)|^2\rangle}{dt} \tag{3}$$

where d is the dimension of the system. As the fluid is confined between parallel plates we measure diffusion in the $x-y$ direction. This means that mean square displacement is given by $\langle|\mathbf{r}_i(t)-\mathbf{r}_i(t_0)|^2\rangle = \langle(x_i(t)-x_i(t_0))^2+(y_i(t)-y_i(t_0))^2\rangle$ and d is set to 2.

III. RESULTS AND DISCUSSION

A. Equation of state of bulk water and methanol

The first step in our study was to obtain an equation of state $\mu(p)$ for the pure substances in bulk. As we will see later, water adsorbs within the studied carbon slit pores at pressures higher than saturation and, thus, it is desirable to have an equation that relates the chemical potential (which is fixed in the GCMC simulations) with pressure, which is one of the experimentally accessible quantities. As mentioned in Section II, we performed two sets of simulations to that aim.

First, we performed hybrid GCMC/MD simulations at specific values of μ along the room temperature isotherm (298 K). The evolution of the density of bulk water and bulk methanol along this isotherm is shown in the top panels of Fig 1. Both sets of data can be accurately fitted to quadratic polynomials. In particular, for water we obtained $\mu(\rho) = -10.214 - 13.091\rho + 11.689\rho^2$ and for methanol $\mu(\rho) = 46.69253 - 150.974\rho + 99.759\rho^2$, where density is expressed in g/cm^3 and μ in $kcal/mol$, as given by LAMMPS.

Next we performed a set of NVT-MD simulations at some values of density within the range covered by the first set of GCMC/MD simulations, from which the equilibrium pressure was estimated through the virial route. The variation of the pressure with density along the room temperature isotherm for water and methanol is shown in the central panels of Fig 1. Again both curves can be fitted to quadratic polynomials, namely, $p(\rho) = 49294 - 11984\rho + 70565\rho^2$ for water and $p(\rho) = 30855.305 - 89217.392\rho + 63615.436\rho^2$ for methanol, where pressure is in atm and density is again in g/cm^3. Using the fits of $\mu(\rho)$ and $p(\rho)$ it is possible to determine the sought equation relating chemical potential and pressure.

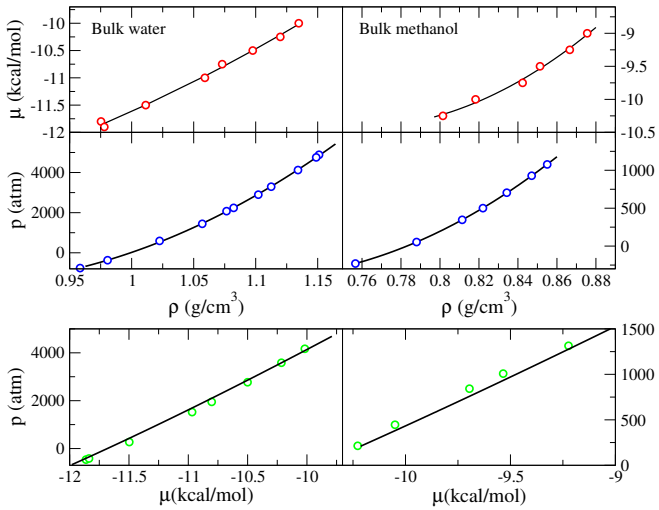

FIG. 1. Simulation data used to obtain the EoS for bulk water (left) and methanol (right) along the room temperature isotherm. Symbols in the top panels show the evolution of density with chemical potential as obtained from hybrid GCMC-MD simulations, middle panels depict density vs pressure as estimated from NVT MD simulations. These results are combined in the bottom panels to express chemical potential as a function of pressure. Continuous curves in the top and middle panels are polynomial fits to the simulation data, whereas in the bottom panel the curve represents the evolution of pressure with chemical potential as obtained from thermodynamic integration (Eq. 7).

The equilibrium pressures corresponding to the selected chemical potentials used in the GCMC/MD simulations are shown as symbols in the lower panels of Fig 1 for water and methanol. Fitting these data we get:

$$p(\mu) = 39636 + 4483.6\mu + 93.384\mu^2 \tag{4}$$

for water and

$$p(\mu) = 14939.66 + 1846.226\mu + 55896\mu^2 \tag{5}$$

for methanol.

With the aim of assessing the reliability of our simulations we have also checked the thermodynamic consistency of $\mu(p)$ (Eqs. (4) and (5)). Helmholtz's free energy can be straightforwardly computed if the chemical potential and pressure are known at a given density and temperature using[41,46]:

$$\frac{A}{Nk_BT} = \frac{\mu}{k_BT} - \frac{p}{\rho k_BT} \tag{6}$$

Once the Helmholtz's free energy is known for a given thermodynamic state $A(\rho_1, T)$, its value for any other state at the same temperature can be calculated by thermodynamic integration (as long as the integration path does not cross any phase transition) using the relation:

$$\frac{A(\rho_2, T)}{N k_b T} = \frac{A(\rho_1, T)}{N k_b T} + \int_{\rho_1}^{\rho_2} \frac{p(\rho)}{k_B T \rho^2} d\rho. \tag{7}$$

Results of the chemical potential evaluation along the 1 atm isobar using thermodynamic integration are shown as continuous lines in the lower panels of Fig 1. As initial conditions, the states with the lowest chemical potential have been used. It is readily apparent from the figures that the chemical potential calculated by thermodynamic integration or from the two sets of hybrid GCMC/MD and NVT MD simulations agree well, which evidences the reliability of our results.

B. Adsorption of water, methanol and their mixtures in graphite slit pores

The adsorption isotherms of the pure substances at room temperature are shown in Fig 2 for the three pore sizes considered. Chemical potentials were transformed into pressures using the EoS given by Eq. (4) for water and the ideal gas law for methanol. Pressures are expressed in terms relative to the saturation vapor pressure, which at 298 K is 7.768×10^{-3} atm for TIP4P/2005 water[35] and 0.09968 atm for OPLS/2016 methanol[33]. For the widest pore (H=15 Å) the adsorption isotherm of water was also estimated using GCMC simulations with the RASPA code[49,50]. The good agreement of the results from both codes gives us confidence on the reliability of the hybrid GCMC/MD simulations performed with LAMMPS.

The first observation is that water adsorption isotherms present a sharp discontinuity for all pore sizes. This behavior has already been reported in previous works[11,12]. These studies have also shown that water adsorption/desorption in graphite slit pores within this range of pore sizes exhibits strong hysteresis, so that the precise location of the vapor-liquid coexistence requires the evaluation of the free energy of the competing phases or the use of more sophisticated simulation techniques such as Gibbs Ensemble simulations. These calculations are beyond the scope of our work. Our goal here is to produce a rough estimate of the pressures at which water is adsorbed into slit graphite pores and of the density of the adsorbed fluid. Simple GCMC simulations similar to ours have been shown

to reproduce rather accurately the hysteresis that has also been experimentally observed in these systems[51]. Therefore, we are confident on the adequacy of our approach.

We found that the onset adsorption pressure is above saturation for all pore sizes considered, i.e. our simulations predict that water does not exhibit capillary condensation in slit graphite pores within the pore sizes considered in this work (7 Å <H < 15 Å), being only adsorbed by applying hydraulic pressure. In particular, the onset pressures obtained in our simulations increase with pore size, adopting the values p≈1200 atm for H=7 Å, p≈2800 atm for H=10 Å and p≈3500 atm for H=15 Å. These results are in qualitative agreement with simulations by Liu and Monson[11] in which water was modeled using SPC/E model[52] and the graphite pore was built with two flat structureless surfaces interacting with the adsorbate via the 10-4-3 Steele potential[53]. These authors reported that water adsorption occurs at relative activities a/a_0 between 1 and 4 for pore sizes within 6.5 Å < H < 16 Å. Expressing our results also as relative activities, our simulations predict that water molecules adsorb at a/a_0 between 1.5 (at H=7 Å) and 8 (at H=15 Å). The quantitative differences might be attributed to the use of different models for both water and the slit pore. Indeed, in the same work, Liu and Monson showed that other water models, such as SPC, predict capillary condensation in narrow pores (6.5 Å < H < 8.8 Å), adsorbing after saturation only in wider pores. Our estimates of the onset pressure in slit graphite pores are of the same order of magnitude as those found in other hydrophobic absorbents such as pure silica MEL or MFI zeolites[38,48,54], whose structure is characterized by intersecting cylindrical pores with effective diameters in the range 5-5.5 Å. Note that some experimental works found adsorption of water in MFI at pressures below the bulk vapor saturation pressure, a fact that is often attributed to the presence of silanol defects in the zeolites[48,55]. The fact that the onset adsorption pressure is lower for the narrowest pores might at first look a bit counter-intuitive, but it is a consequence of the stronger energetic interactions between the walls and the layer of adsorbed water. The hydrophobicity of the pore does not imply a net adsorbate-adsorbent repulsion, it simply reflects that adsorbate-adsorbate interactions are stronger than those between adsorbate and the pore walls. But once water adsorption is forced by pressure, the attraction between adsorbate molecules and the pore walls is larger for small pore sizes (where molecules interact strongly with both walls) that for wider pores. This explains why onset adsorption pressures increase with pore size in the nanometer range.

Finally, it is evident from Fig. 2 (top panel) that the density of the adsorbed fluid at a given pressure increases with pore size. For example, the density of adsorbed water at the specific pressure p≈3500 atm (the onset adsorption pressure for the widest pore) goes from about 0.912 g/cm^3 for H=7 Å to 1.000 g/cm^3 at H=10 Å, and to 1.051 g/cm^3 for H=15 Å. This is to be compared to 0.997 g/cm^3 for bulk water at ambient conditions. Note, however, that the density of a fluid under nano-confinement is not a well defined quantity, as it is strongly affected by the criterion that defines the effective pore volume. This quantity is determined by the accessible pore volume, which in turn depends on the size and shape of the adsorbate molecules. Except for very small adsorbates (e.g. Ar), density comparisons between bulk and confined fluids can only be qualitative. In any case, the relatively low density of water adsorbed in the narrowest pore, clearly reflects the substantially smaller coordination number of the molecules adjacent to the walls (most of them). As pore width increases, the density of the adsorbed phase increases as well, reflecting the higher average molecular coordination as the ratio of molecules close to the walls drops.

Focusing now on methanol (Fig. 2 (bottom panel)), our simulations indicate that the onset adsorption pressure also increases with pore size, but, differently from water, it is well below bulk saturation pressure for all pore sizes considered in this work. The size dependence of the onset adsorption pressure can be explained in the same terms as that exhibited by water, but now the adsorption process is energetically slightly more favored due to the preference of the non-polar tails of the alcohol molecules for the graphite walls. Due to this dominance of the methyl group-graphite interaction and the less energetic methanol-methanol interaction with respect to than between water molecules, adsorption starts below saturation pressure, and no hydraulic pressure needs to be applied. Another remarkable difference between both adsorbates is the fairly smooth shape of the methanol adsorption isotherm, i.e., the density grows steadily over a finite range of pressures until saturation without marked jumps. One evident trend is that the largest the pore, the more abrupt is the condensation transition within the pore (even exhibiting hysteresis). This agrees with type IV-V adsorption isotherms, typical of adsorption into mesopores when there is condensation[56]. For pore widths under 10 Å (15 Å for methanol) the transition is smeared out, as finite size effects emerge and we no longer have a proper thermodynamic transition. Under these tight confinement conditions the adsorption behavior leads to a type I adsorption isotherm, characteristic of adsorption into micropores[56]. Finally, saturation is reached

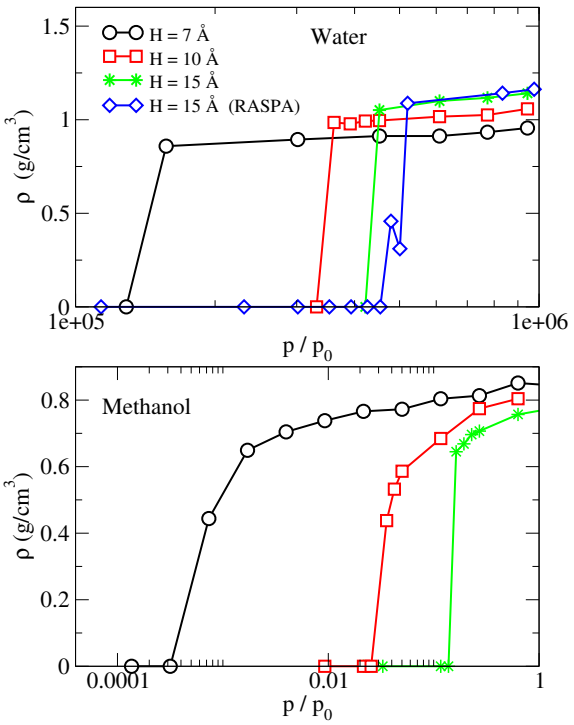

FIG. 2. Adsorption isotherm of pure water (top panel) and methanol (bottom panel) in a slit graphite pore as a function of pore width at 298 K.

for higher pressures as the pore sizes increase, leading to a similar confined fluid density ≈ 0.8 g/cm^3 in all cases. This is practically the density of bulk liquid methanol at ambient conditions (0.792 g/cm^3). The onset adsorption pressures obtained in this work are somewhat lower than those reported in previous simulation studies using the TraPPE model[57] for methanol[24]. In particular, our simulations predict that methanol starts to adsorb at $p \approx 7 \times 10^{-5}$ atm. for H=7 Å, at $p \approx 0.0035$ atm for H=10 Å, and at $p \approx 0.0163$ atm for H=15 Å, to be compared to $p \approx 0.00059$ atm for H=8 Å, $p \approx 0.0051$ atm for H=10 Å, and $p \approx 0.0278$ for H=16 Å reported in Ref. 24. These discrepancies can be attributed to the larger value of the ϵ LJ parameter of the OPLS/2016 compared to that of TraPPE potential. This gives rise to a more intense methanol-wall attraction that obviously would shift the onset adsorption pressure to lower values. On the other hand, our results are consistent with the fact that methanol adsorption into other hydrophobic adsorbents, such as pure silica zeolites, also occurs below bulk saturation pressure[38,48].

In the case of water-methanol mixtures, adsorption was studied from the vapor phase in equilibrium with a liquid solution at a given concentration. The study was performed

at three different compositions of the liquid mixture, going from the dilute (x^l_{MeOH}=0.020), low concentration (x^l_{MeOH}=0.115), and finally to high alcohol concentration (x^l_{MeOH}=0.692) regimes. The density of the adsorbed fluid as well as its composition as a function of the composition of the bulk liquid phase and pore width are presented in Table III. Even though the pressures considered here are much lower than those of the onset adsorption of pure water, our results indicate that water molecules are always adsorbed for all pore sizes. This is explained by the fact that water molecules can co-adsorb with methanol in highly hydrophobic pores due the formation of hydrogen bonds with previously adsorbed alcohol molecules. This phenomenon has already been reported in water/alcohol adsorption in other hydrophobic porous materials such as pure silica zeolites[38,48]. In any case, alcohol adsorbs preferentially over water for all pore sizes compositions studied here. Note that the highly dilute mixture is not adsorbed into the largest pore H=15Å. This apparently strange result stems from the fact that the partial pressure of methanol in this liquid solution ($x^l_{MeOH} = 0.02$) is very low, $p \approx 5 \times 10^{-3}$ atm, actually below the onset adsorption pressure of pure methanol for the corresponding pore size ($p \approx 0.016$ atm). Since methanol molecules will not then be able to enter the pore, the same will happen to water. In the remaining cases, the concentration of methanol in the confined fluid is always above 60%, reaching a maximum of 95% for the fluid adsorbed in the narrowest pore in equilibrium with the highly concentrated solution. Our results evidence a clear trend in the adsorption behavior: the concentration of adsorbed methanol increases as the pore width narrows, and when the alcohol concentration of the bulk liquid solution increases. These results are consistent with another recent simulation study in which the adsorption of alcohol/water mixtures at a mole fraction of 5% in slit graphene pores 20Å-wide is modeled using SPC/E water and OPLS-AA alcohol[21]. In that instance, an alcohol concentration close to 91% for the adsorbed methanol-water mixture was reported, in agreement with our findings. Note, however, that the study of Gao et al.[21] is not directly comparable to ours, since in their case the confined fluid is not in equilibrium with a liquid solution mediated by the corresponding vapor phase, i.e., it is not the result of an equilibrium adsorption process.

x^l_{MeOH}	x^g_{MeOH}	p (atm.)	x^a_{MeOH}			$\rho^a_{H_2O}/\rho^a_{MeOH}$		
			H=7Å	H= 10Å	H=15Å	H=7Å	H= 10Å	H=15Å
0.020	0.144	0.03525	0.87(5)	0.63(2)	—	0.0016/0.014	0.0058/0.0104	—
0.115	0.504	0.05605	0.92(3)	0.80(2)	0.79(2)	0.0011/0.015	0.0031/0.0131	0.0033/0.0123
0.692	0.882	0.1296	0.95(2)	0.87(3)	0.86(1)	0.0006/0.015	0.0021/0.0145	0.0022/0.0135

TABLE III. Concentration of adsorbed methanol (x^a_{MeOH}) in slit graphite pores as a function of the mixture concentration of the liquid solution and pore size. Liquid-vapor equilibrium conditions were taken from experiments[47]. Number densities are given in molec./Å^3 units.

C. Structural properties of adsorbed fluids

Number density profiles of the adsorbed fluids along the axis perpendicular to the graphite walls are provided in Fig. 3. For pure substances, density profiles were calculated at the equilibrium density corresponding to the onset adsorption pressure for the widest pore: p≈3500 atm (p/p_0=4.5×10^5) in the case of water, and p≈0.063 atm (p/p_0=0.63) for methanol. As it is evident from Fig. 3, oxygen atoms of water are arranged into layered structures for the three pore sizes studied, the number of layers increasing from one at H=7 Å to two at H=10 Å to four at H=15 Å. Water hydrogen atoms profiles exhibit the highest peaks at the same locations as oxygen atoms, but in this case smaller peaks emerge on both sides of the higher peaks. The smaller hydrogen peaks between two oxygen layers are visibly more intense than those that appear close to the pore walls. For the narrowest pore, in which one single water layer is formed, water molecules are mostly oriented parallel to the walls, so that they can form hydrogen bonds within the layer plane. In any case, out-of-plane vibrations are also present, as evidenced by the appearance of two smaller peaks close to the walls. These features are also clearly visible in instantaneous snapshots of the system viewed from the directions perpendicular (Fig. 4) or parallel (Fig 5) with respect to the walls. In pores of size H=10Å, hydrogen peaks close to wall decrease and a clear peak between the oxygen layers appears, indicating that hydrogen bonds are formed not only within but also across layers. The same occurs for H=15Å, but in this case the two inner layers are closer to each other and less defined, with a much larger number of hydrogen bonds between them.

The tendency to form layered structures is also evident in the case of methanol. The

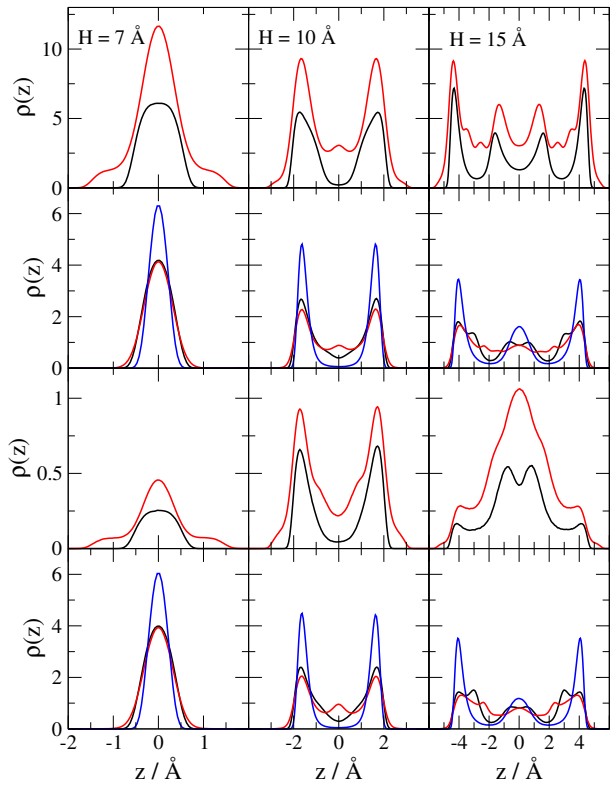

FIG. 3. Top two rows: density profiles of adsorbed pure water (first row) and methanol (second row) in slit graphite nanopore at constant temperature T = 298 K and constant density corresponding to the equilibrium adsorbed density at the onset adsorption pressure for the H=15 Å pore, p≈3500 atm for water and p≈0.0036 atm for methanol. Two bottom rows: density profiles of adsorbed water (third row) and methanol (fourth row) from a liquid mixture with methanol molar fraction x^{l}_{MeOH}=0.115 (corresponding to x^{a}_{MeOH}=0.92(3) for the adsorbed fluid) at 298 K and vapor-liquid equilibrium pressure. Black line represents density of oxygen atoms, red line of hydrogen and blue line of methyl group.

difference is that due to the larger size of the methyl group only three layers are formed in the widest pore H=15 Å. Another remarkable difference is that oxygen and hydrogen atom profiles are almost identical for the narrowest pore H=7 Å, which indicates that hydrogen vibrations are now much more restrained. The reason is that each methanol molecule can only be involved in two hydrogen bonds and these two bonds are better preserved in a planar configuration. As a consequence, hydrogen atoms lie nearly on the same plane as the oxygen atoms. Due to its larger size, the location of the methyl group is even more restrained, with its distribution exhibiting a higher and narrower peak. These two features force methanol

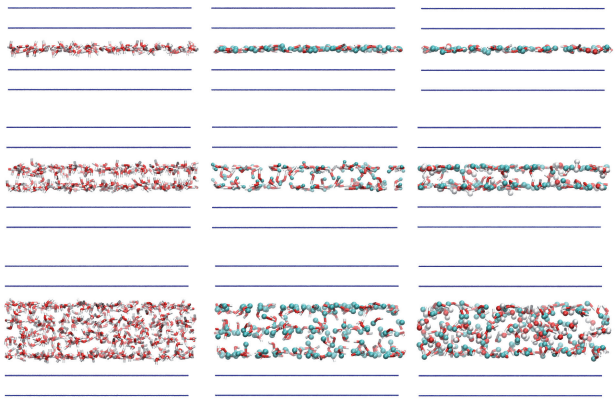

FIG. 4. Side view of instantaneous configurations of pure water (left column), pure methanol (middle column) and an alcohol-water mixture (right column) confined in slit graphite pores of width H=7 Å (first row), H=10 Å (second row), and H=15 Å (third row) at 298 K. Densities of confined fluids correspond to p≈3500 atm (p/p_0=4.5×10^5) for water, at p≈0.0036 atm (p/p_0=0.63) for methanol and at p≈0.05605 atm for the mixture adsorbed in equilibrium with a bulk liquid solution with x^l_{MeOH}=0.115.

molecules to be oriented parallel to the pore walls. Indeed, as seen in Fig. 5, methanol molecules tend to form long hydrogen bond chains. When two or more layers are formed, though, peaks between the oxygen-methyl maxima again appear, indicating that inter-layer hydrogen bonds are formed between layers (Fig. 4). As three layers are formed, oxygen peaks are split into two very close maxima, which might be attributed to the fact that both intra-layer and inter-layer hydrogen bonds are nearly equally likely.

Let us now focus on water/methanol solutions. Since the concentration of the adsorbed methanol/water mixture is relatively similar for the three bulk liquid mixtures considered in this work, for the sake of brevity, density profiles are only shown for the bulk molar fraction x^l_{MeOH}=0.115. The density profiles of methanol remain almost unchanged with respect to those of the pure substance (Fig. 3), due to the fact that the adsorbed water/alcohol mixture is highly concentrated in alcohol. The same is true for the atomic distributions of water in the narrowest pore, but in this case, because geometric constrains are too tight. As can be seen in Fig. 5, methanol molecules form chain-like structures very similar to those found in the pure system, only with a slightly higher tendency to form branched chains due to the presence of water molecules that have more sites available for H-bonds. However, whenever

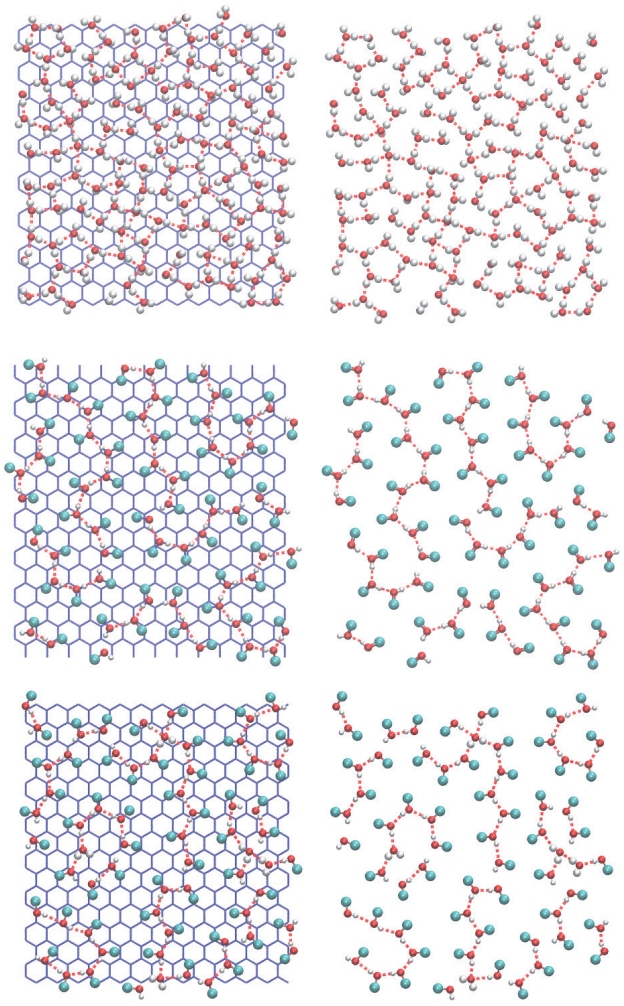

FIG. 5. Top view of instantaneous configurations of pure water (left row), pure methanol (middle row) and water-methanol mixture (right row) adsorbed in slit graphite pores with H=7 Å at 298 K. In the second row the underlying graphite plane has removed to aid the visualization of the adsorbed fluid. Density of confined fluid correspond to p≈3500 atm (p/p_0=4.5×10^5) for water, at p≈0.0036 atm (p/p_0=0.63) for methanol and at p≈0.05605 atm in equilibrium with a bulk liquid mixture with x^l_{MeOH}=0.115.

two and specially three layers are formed, there is a clear tendency of water molecules to be shifted towards the central region of the pore. This is evidenced in the asymmetric shape of the peaks of the oxygen atom distribution in the two layer instance. One can appreciate that the inner side of the peak becomes broader. In the three layer case there is a sudden enhancement/depression of the inner/outer oxygen and hydrogen peaks. Obviously, the

highly hydrophobic character of the graphite walls and their affinity towards the non-polar alcohol tails explains this behavior. These structural features have already been reported in previous simulation studies for wider pores[20,21].

D. Diffusion under confinement

Diffusivities of pure substances were computed at the same thermodynamic states as the density profiles presented in the previous section, i.e., at the onset pressure of water for the widest pore, $p \approx 3500$ atm (p/p_0=4.5×10^5), and $p \approx 0.063$ atm (p/p_0 =0.63) for methanol. The corresponding mean square displacements (MSD) are plotted in Fig. 6.

Diffusion of fluids can occur through several mechanisms that are characterized by different scalings of the evolution of the mean square displacement with time, namely

$$\langle |x_i(t) - x_i(t_0)|^2 + |y_i(t) - y_i(t_0)|^2 \rangle \propto t^k, \tag{8}$$

where the value of k depends on the diffusion mechanism. Diffusion of bulk water and methanol at long times occurs through a Fickian mechanism in which the mean square displacement scales linearly with time. At short times molecules exhibit a rather coordinated movement that leads to a quadratic scaling of the MSD, in what is known as the ballistic regime. Previous studies showed that confined water also exhibits Fickian diffusion even when confined in narrow pores[3], although other studies report a single-file mechanism in narrow pores, according to which MSD scales with the square root of time (see, for example, Ref. 20). As it is evident from Fig.6, our simulations predict that diffusion of adsorbed pure water follows a Fickian mechanism even in the narrowest pore H=7 Å. This is in disagreement with the results of Zhao and Yang[20], who report single-file diffusion for water adsorbed in the H=7 Å pore. Note, however, that Zhao and Yang used a different water model, SPC/E, and studied a somewhat higher density (0.03337 molec./Å^3 vs 0.0306 molec./Å^3 in our simulations). Further work is needed to clarify the origin of this discrepancy. On the other hand, for wider pores, Zhao and Yang[20] predict Fickian diffusion in agreement with our results. Regarding pure methanol, its MSD is shown in Fig 6. In this case, diffusion is also Fickian in the wider pores. In contrast, for the narrowest pore it exhibits a sub-diffusive behavior ($k < 0.5$). Indeed methanol molecules did not diffuse at all during the time scale of our simulations, which can be ascribed to the large size of the methyl group. This is

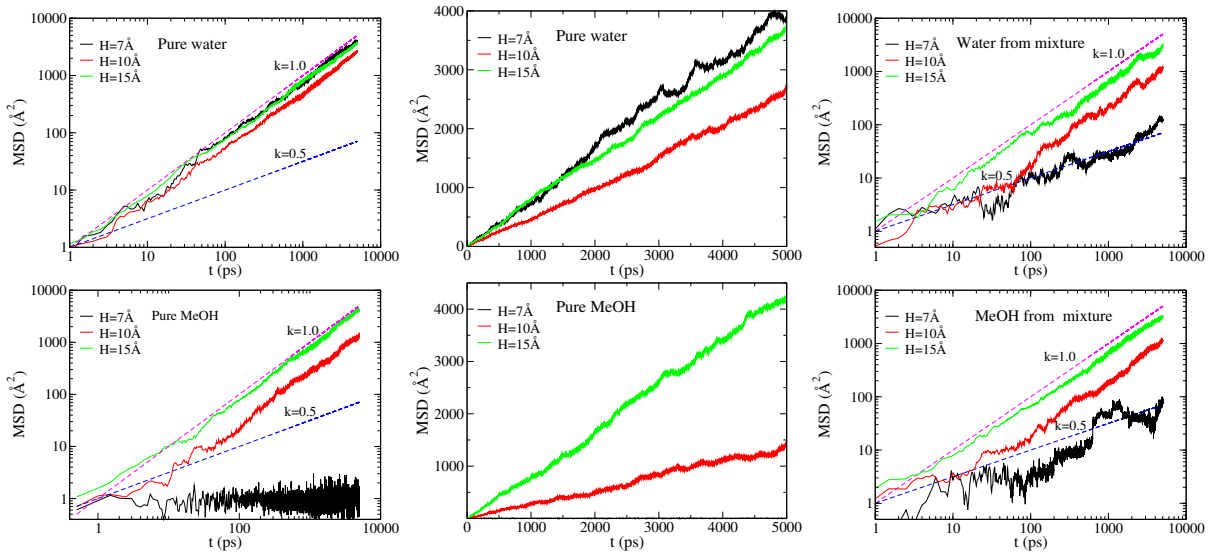

FIG. 6. Lateral mean square displacement of adsorbed water (top row) and methanol (bottom row) in slit graphite pores for the three considered pore sizes at T=298 K. Pressure was set to saturation value in the widest pore for the pure components (p ≈3500 atm for water and p ≈0.063 atm for methanol), and to liquid-vapor equilibrium conditions for the mixtures. Left and central panels show the diffusion of adsorbed pure fluids in logarithm and linear scale, respectively, and right panels show the diffusion of water and methanol adsorbed from a x^l_{MeOH}=0.115 mixture. Dotted blue and purple lines show the expected behavior for Fickian (k=1) and single-file (k=0.5) diffusion mechanisms.

also at odds with previous results of ethanol confined in H=7Å pores, in which ethanol was found to undergo single-file diffusion. Since ethanol molecules are larger than methanol ones, one would expect that ethanol diffusion would be slower, which is actually the case in the bulk[30,58]. A possible explanation for this discrepancy is the disparity of models used to describe the alcohols. Methyl group is modeled with a slightly larger size in the OPLS/2016 parameterization (σ_{CH_3}=3.6499 Å) used in this work than that of OPLS-AA (σ_{CH_3}=3.5 Å) of Ref. 20. We speculate that this non-negligible difference in the size of the methyl group might be enough to prevent the displacement of methanol molecules.

Diffusion coefficients of confined pure substances, which were calculated using Eq. (3), are given in Table IV and plotted in Fig. 7 together with the corresponding values of the bulk liquid at ambient conditions (as predicted by TIP4P/2005[36] and OPLS/2016[33] models). The diffusion constant of confined water presents a non-monotonic dependence on pore size,

exhibiting a minimum for H=10 Å. Interestingly, the diffusion of confined water in pores with H=7 Å has value similar to that of the bulk system. For H=10 Å undergoes an abrupt drop to less than half its value, and at H=15 Å increases again. Previous simulation studies have shown that water presents a non-monotonous variation with pore size when confined in quartz and graphite pores, which is related to the freezing and melting of the adsorbed water bilayer[59,60]. These works predict a drop of the diffusion constant of up to four orders of magnitude, evidencing the fluid-solid-fluid transition. This behavior is not observed in our simulations, because only three pore sizes were considered, namely, H=7, 10 and 15 Å, and this phenomenon has been reported to occur at H=9-9.5 Å for TIP4P/2005[14,60]. On the other hand, we can think that the abnormally high value of water diffusivity for the small pore size is the result of the small coordination number of the water molecules, that in this highly confined situation are forced to be structured in an almost planar layer, as previously commented. Increasing the pore size transforms the bidimensional network of H-bonds into a three dimensional one, that necessarily hampers the molecular motion. It might actually be the case that the vicinity of a potential fluid-solid transition might aid in a further reduction of the diffusivity. For larger pores, the diffusion constants reach values slightly below that of the bulk. The fact that the both density and diffusivity increase when going from 10 Å to 15 Å, which is apparently conflicting, might also be connected with the well known diffusivity anomaly of water[4].

In the case of methanol, aside from the narrowest pore in which methanol displacement is severely hampered, diffusion exhibits a monotonous behavior in which the diffusion constant increases with pore size. Note that in this case case the diffusion constant of methanol is much lower than that of the bulk liquid at room conditions.

The evolution of the lateral MSD of water and methanol in the adsorbed mixtures is presented in Fig. 6. The first observation for the competitive diffusion is that both water and methanol exhibit a single-file mechanism in the narrowest pore H=7 Å, whereas diffusion is again Fickian for the largest pore sizes. The radical change in the diffusion behavior of both components in the narrowest pore indicates that movements of water and methanol molecules are strongly coupled. Note that the diffusion of pure methanol was completely hindered in the narrowest pore, but now in the presence of water, methanol is able to diffuse into the pore. Visual inspection of the simulation trajectories reveals that the reason for this behavior lies in the ability of water molecules to diffuse due to their smaller size. The

	D_{H_2O}/D_{MeOH}			ρ_{H_2O}/ρ_{MeOH}		
x^l_{MEOH}	H=7 Å	H=10 Å	H=15 Å	H=7 Å	H=10 Å	H=15 Å
Pure system	2.0/–	0.7/0.4	1.8/1.1	0.0306/0.0143	0.0333/0.0151	0.0354/0.0141
0.144	$1.1\ 10^{-1}/1.1\ 10^{-1}$	2.1/1.5	—-	0.0016/0.014	0.0058/0.0104	—
0.505	$1.2\ 10^{-2}/1.7\ 10^{-2}$	0.8/0.7	1.7/1.9	0.0011/0.015	0.0031/0.0131	0.0033/0.0123
0.882	$1.7\ 10^{-2}/2.5\ 10^{-2}$	1.3/1.4	1.8/1.1	0.0006/0.015	0.0021/0.0145	0.0022/0.0135

TABLE IV. Diffusion coefficients of pure water, methanol and their mixtures confined in graphite slit pores as a function of pore size and composition at T=298 K, in 10^{-9} m^2/s units. Pressure was set to saturation value in the widest pore for the pure components ($p \approx$3500 atm for water and $p \approx$0.063 atm for methanol), and to liquid-vapor equilibrium conditions for the mixtures. Average number densities of the water and methanol in the confined phase are given in molec./Å^3.

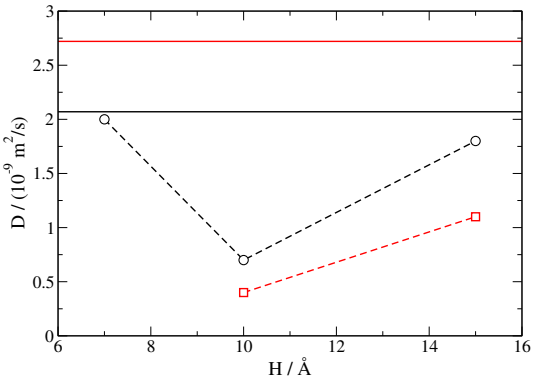

FIG. 7. Diffusion of pure water (black circles) and pure methanol (red squares) confined in slit graphite pores as a function of pore size at T=298 K and at the onset pressure of each component in the widest pore ($p \approx$3500 atm for water and $p \approx$0.063 atm for methanol). Values of the bulk systems at room pressure and temperature are shown as solid lines (water in black and methanol in red).

strong water-methanol hydrogen bonding is able to break the chain-like methanol clusters, and thus aid the diffusion of methanol molecules thanks to this cooperative mechanism. Diffusion constants of water and methanol in the mixtures are collected in Table IV. For all pore sizes and compositions methanol and water diffusion constants present similar values, reinforcing the idea that water and methanol movements are coupled. The tendency of water and alcohol to form clusters and diffuse together has already been pointed out in the work of

Krishna and van Baten[61]. On the other hand, the dependence of the diffusivity on pore size for a given bulk liquid composition follows the expected trend, i.e. diffusivity increases with pore size. It is also observed that for a given pore size, diffusivity decreases with increasing alcohol concentration of the bulk solution in equilibrium with the pore. This can be related to the fact that the ratio of water in the mixture is lowered, and therefore there are less water molecules available to promote methanol diffusion.

IV. SUMMARY AND CONCLUSIONS

The adsorption of water, methanol and their mixtures in slit graphite pores has been investigated by molecular simulations. The influence of pore size and composition of the bulk liquid mixture in equilibrium with the confined (adsorbed) fluid were investigated. Our simulations indicate that, in agreement with previous simulation studies, water does not undergo capillary condensation in these hydrophobic slit pores in the nanometer range. Actually, its adsorption requires the application of hydraulic pressure. On the contrary, methanol is adsorbed before the bulk saturation pressure for all pore sizes. In both pure substances onset adsorption pressure increases with pore size. Concerning alcohol/water mixtures, we have found that for all bulk liquid solution compositions, alcohol adsorbs preferentially over water. Alcohol concentration in the adsorbed mixture is largest for small pores and when the adsorption takes place from highly concentrated solutions.

Analysis of the structure of the adsorbed fluid shows that water and methanol tends to form layered structures, with the number of layers obviously increasing with pore size. The largest pore can fit four water layers but only three methanol layers due to the larger size of the methyl group. For mixtures, density profiles of methanol and water show that, as expected for hydrophobic walls, alcohol tend to occupy positions close to the walls displacing water towards the pore center. The study of diffusion under confinement reveals a rather peculiar behavior. For pure substances, water diffuses faster than methanol at all pore sizes, differences being specially large in the narrowest pore, in which water diffuses almost as in bulk, whereas methanol diffusion is practically negligible. Surprisingly, methanol is able to diffuse in the narrowest pores by the addition of small amounts of water. In this case water and methanol present similar diffusivities, which indicates a coordinated movement of both components. Indeed, water and methanol exhibit rather similar diffusion constants for all

pore sizes and liquid compositions, reinforcing the idea of a coupled diffusion mechanism. This is an important result, as it indicates that narrow hydrophobic pores can be good candidates for water/methanol separation based on equilibrium adsorption. On one hand they provide the better equilibrium water/alcohol selectivity and, on the other, the diffusion might not be as slow as one would expect, since the presence of even tiny amounts of water molecules suffices to enhance methanol mobility.

Future work will focus on the extension of this analysis to hydrophilic and mixed hydrophobic/hydrophilic walls. This could potentially facilitate the assessment of the best experimental conditions leading to water/alcohol micro-phase separation, an information that can be very relevant for the design of nanoporous materials for alcohol dehydration.

ACKNOWLEDGMENTS

PP is grateful for an Erasmus fellowship that sponsored her stay in Madrid. EGN and EL acknowledge the support from the Agencia Estatal de Investigacin and Fondo Europeo de Desarrollo Regional (FEDER) under grant No. FIS2017-89361-C3-2-P, and partial support from the European Unions Horizon 2020 Research and Innovation Staff Exchange programme under the Marie Skodowska-Curie grant agreement No 734276, and TU thanks the support of the Slovenian Research Agency (P1 0103-0201, N1-0042)

REFERENCES

[1]L. M. Vane, "Separation technologies for the recovery and dehydration of alcohols from fermentation broths," *Biofuels, Bioprod. Bioref.*, vol. 2, pp. 553–588, 2008.

[2]K. Koga, G. T. Gao, H. Tanaka, and X. C. Zeng, "Formation of ordered ice nanotubes inside carbon nanotubes," *Nano Lett.*, vol. 412, pp. 802–805, 2001.

[3]A. Striolo, "The mechanism of water diffusion on narrow carbon nanotubes," *Nano Lett.*, vol. 6, pp. 633–639, 2006.

[4]P. Kumar, S. V. Buldyrev, F. W. Starr, N. Giovambattista, and H. E. Stanley, "Thermodynamics, structure and dynamics of water confined between hydrophobic plates," *Phys. Rev. E*, vol. 72, p. 051503, 2005.

[5]N. Giovambattista, P. J. Rossky, and P. G. Debenedetti, "Phase transitions induced by nanoconfinement in liquid water," *Phys. Rev. Lett.*, vol. 102, p. 050603, 2009.

[6]G. Algara-Siller, O. Lehtinen, F. C. Wang, R. R. Nair, U. Kaiser, H. A. Wu, A. K. Geim, and I. V. Grigorieva, "Square ice in graphene nanocapilaries," *Nature*, vol. 519, p. 443, 2015.

[7]P. Hirunsit and P. B. Balbuena, "Effects of confinement on water structure and dynamics: a molecular simulation study," *J. Phys. Chem. C*, vol. 111, pp. 1709–1715, 2007.

[8]D. Argyris, N. R. Tummala, A. Striolo, and D. R. Cole, "Molecular structure and dynamics in thin water films at the silica and graphite surfaces," *J. Phys. Chem. C*, vol. 112, pp. 13587–13599, 2008.

[9]P. A. Bonnaud, B. Coasne, and R. J.-M. Pellenq, "Molecular simulation of water confined in nanoporous silica," *J. Phys.: Condens. Matter*, vol. 22, p. 284110, 2010.

[10]R. Srivastava, H. Docherty, J. K. Singh, and P. T. Cummings, "Phase transition of water in graphite and mica pores," *J. Phys. Chem. C*, vol. 115, p. 12488, 2011.

[11]J.-C. Liu and P. A. Monson, "Does water condense in carbon pores?," *Langmuir*, vol. 21, p. 10219, 2005.

[12]A. Striolo, A. A. Chialvo, P. T. Cummings, and K. E. Gubbins, "Water adsorption in carbon-slit nanopores," *Langmuir*, vol. 19, p. 8583, 2003.

[13]Z. Gao, N. Giovambattista, and O. Sahin, "Phase diagram of water confined by graphene," *Sci. Rep.*, vol. 8, apr 2018.

[14]J. Dix, L. Lue, and P. Carbone, "Why different models predict different structures under 2d confinement," *J. Comp. Chem.*, vol. 39, no. 25, pp. 2051–2059, 2018.

[15]C. Alba-Simionesco, B. Coasne, G. Dosseh, G. Dudziak, K. E. G. R. Radhakrishnan, and M. Sliwinska-Bartkowiak, "Effects of confinement on freezing and melting," *J. Phys.: Condens. Matter*, vol. 18, pp. R15–R68, 2006.

[16]K. Nomura, T. Kaneko, J. Bai, J. S. Francisco, K. Yasuoka, and X. C. Zeng, "Evidence of low-density and high-density liquid phases and isochore end point for water confined to carbon nanotube," *Proc. Natl. Acad. Sci. U.S.A.*, vol. 114, pp. 4066 – 4071, 2017.

[17]N. Severin, I. M. Sokolov, and J. P. Rabe, "Dynamics of ethanol and water mixtures observed in a self-adjusting molecularly thin slit pore," *Langmuir*, vol. 30, pp. 3455–3459, 2014.

[18]N. Severin, J. Gienger, V. Scenev, P. Lange, I. M. Sokolov, and J. P. Rabe, "Nanophase separation un monomolecularly thin water-ethanol films controlled by graphene," *Nano Lett.*, vol. 15, pp. 1171–1176, 2015.

[19]P. Bampoulis, J. P. Witteveen, E. S. Kooij, D. Lohse, and B. Poelsema, "Structure and dynamics of confined alcohol-water mixtures," *ACSNano*, vol. 10, pp. 6762–6768, 2016.

[20]M. Zhao and X. Yang, "Segregation structures and miscellaneous diffusions for ethanol/water mixtures in graphene-based nanoscale pores," *J. Phys. Chem. C*, vol. 119, p. 21664, 2015.

[21]Q. Gao, Y. Zhu, Y. Ruan, Y. Zhang, W. Zhu, X. Lu, and L. Lu, "Effect of adsorbed alcohol layers on the behavior of water molecules confined in a graphene nanoslit: a molecular dynamics study," *Langmuir*, vol. 33, p. 11467, 2017.

[22]S. Gravelle, H. Yoshida, L. Yoly, C. Ybert, and L. Bocquet, "Carbon membranes for efficient water-ethanol separation," *J. Chem. Phys.*, vol. 145, p. 124708, 2015.

[23]A. Kommu and J. K. Singh, "Separation of ethanol and water using graphene and hexagonal boron nitride slit pores: a molecular dynamics study," *J. Phys. Chem. C*, vol. 121, pp. 7867–7880, 2017.

[24]V. T. Nguyen, D. D. Do, and D. Nicholson, "Microscopic configurations of methanol molecules in graphitic slit micropores: a computer simulation study," *J. Colloid. and Inter. Sci.*, vol. 396, pp. 215–226, 2013.

[25]F. Mozaffari, "Molecular dynamics simulation study on the structure and the dynamic properties of nano-confined alcohols between graphene surfaces," *Fluid Phase Equilib.*, vol. 431, pp. 8–15, 2017.

[26]A. V. Shevade, S. Jiang, and K. E. Gubbins, "Adsorption of water-methanol mixtures in carbon and alumino-silicate pores: a molecular dynamics study," *Molec. Phys.*, vol. 97, pp. 1139–1148, 1999.

[27]T. Ohkubo, T. Iiyama, and K. Kaneko, "Organized structures of methanol in carbon nanospaces at 303k studies with in situ x-ray diffraction," *Chem. Phys. Lett.*, vol. 312, pp. 191–195, 1999.

[28]A. Andreu, H. F. Stoeckli, and R. H. Bradley, "Specific and non-specific interactions on carbon black surfaces," *Carbon*, vol. 45, p. 18541864, 2007.

[29]K. Morishige and K. Mikawa, "Tensile effect on crystal nucleation of methanol and ethanol confined in pores," *J. Phys. Chem. C*, vol. 116, pp. 3618–3622, 2012.

[30]Z. J. Derlacki, A. J. Easteal, A. V. J. Edge, L. A. Woolf, and Z. Roksandic, "Diffusion coefficients of methanol and water and the mutual diffusion coefficient in methanol-water solutions at 278 and 298 k," *J. Phys. Chem.*, vol. 89, pp. 5318–5322, 1985.

[31]K. R. Harris, P. J. Nevitt, and Z. J. Derlacki, "Alcohol tracer diffusion, density, nmr and ftir studies of acqueous 2,2,2-trifluoroethanol solutions at 25 c," *J. Chem. Soc.: Faraday Trans.*, vol. 94, pp. 1963–1970, 1998.

[32]J. L. F. Abascal and C. Vega, "A general purpose model for the condensed phases of water: Tip4p/2005," *J. Chem. Phys.*, vol. 123, p. 234505, 2005.

[33]D. González-Salgado and C. Vega, "A new intermolecular potential for simulations of methanol: The opls/2016 model," *J. Chem. Phys.*, vol. 145, p. 034508, 2016.

[34]D. González-Salgado, K. Zemankova, E. G. Noya, and E. Lomba, "Temperature of maximum density and excess thermodynamics of aqueous mixtures of methanol," *J. Chem. Phys.*, vol. 144, p. 184505, 2016.

[35]C. Vega, J. L. F. Abascal, and I. Nezbeda, "Vapor-liquid equilibria from the triple point up to the critical point for the new generation of tip4p-like models: Tip4p/ew, tip4p/2005, and tip4p/ice," *J. Chem. Phys.*, vol. 125, p. 034503, 2006.

[36]C. Vega, J. L. F. Abascal, M. M. Conde, and J. L. Aragonés, "What ice can teach us about water interactions: a critical comparison of the performance of different water models," *Faraday Discuss.*, vol. 141, pp. 251–276, 2009.

[37]M. Mijaković, K. D. Polok, B. Kežić, A. Perera, and L. Zoranić, "A comparison of force fields for ethanol-water mixtures," *Mol. Sim.*, vol. 41, pp. 699–712, 2015.

[38]P. Gómez-Álvarez, E. G. Noya, E. Lomba, S. Valencia, and J. Pires, "Study of short-chain alcohol and alcohol-water adsorption in mel and mfi zeolites," *Langmuir*, vol. DOI:10.1021/acs.langmuir.8b02326, 2018.

[39]D. Feller and K. D. Jordan, "Estimating the strength of the water/single-layer graphite interaction," *The Journal of Physical Chemistry A*, vol. 104, pp. 9971–9975, nov 2000.

[40]T. Werder, J. H. Walther, R. L. Jaffe, T. Halicioglu, and P. Koumoutsakos, "On the water-carbon interaction for use in molecular dynamics simulations of graphite and carbon nanotubes," *J. Phys. Chem. B*, vol. 107, pp. 1345–1352, feb 2003.

[41]D. Frenkel and B. Smit, *Understanding Molecular Simulation. From Algorithms to Applications*. Boston: Academic Press, 1996.

[42]S. Plimpton, "Fast parallel algorithms for short-range molecular dynamics," *J. Comp. Phys.*, vol. 117, pp. 1–19, 1995.

[43]F. R. Hockney and J. Eastwood, *Computer Simulation Using Particles*. Adam Hilger, 1988.

[44]S. Nose, "A unified formulation of the constant temperature molecular dynamics methods," *J. Chem. Phys.*, vol. 81, pp. 511–519, 1984.

[45]W. G. Hoover, "Canonical dynamics:equilibrium phase-space distributions," *Phys. Rev. A: At., Mol., Opt. Phys.*, vol. 31, pp. 1695–1697, 1985.

[46]C. Vega, E. Sanz, J. L. Abascal, and E. G. Noya, "Determination of phase diagrams by computer simulation: methodology and applications to water, electrolytes and proteins," *J. Phys. Cond. Mat.*, vol. 20, p. 153101, 2008.

[47]J. Gmehling and U. Onken, *Vapor-Liquid equilibrium Data Collection. Aqueous-Organic Systems*. Dechema Chemistry Data Series, Vol. I, Part 1, Dechema, 1977.

[48]P. Bai, M. Tsapatsis, and J. L. Siepmann, "Multicomponent adsorption of alchols onto silicalite-1 from aqueous solution: isotherms, structural analysis, and assessment of ideal adsorbed solution theory," *Langmuir*, vol. 28, pp. 15566–15576, 2012.

[49]D. Dubbeldam, S. Calero, D. E. Ellis, and R. Q. Snurr, "Raspa: molecular simulation software for adsorption and diffusion in flexible nanoporous materials," *Mol. Simul.*, vol. 42, pp. 81–101, 2016.

[50]D. Dubbeldam, A. Torres-Knoop, and K. S. Walton, "On the inner workings of monte carlo codes," *Mol. Simul.*, vol. 39, pp. 1253–1292, 2013.

[51]L. Sarkisov and P. A. Monson, "Hysteresis in monte carlo and molecular dynamics simulations of adsorption in porous materials," *Langmuir*, vol. 16, p. 9857, 2000.

[52]H. J. C. Berendsen, J. R. Grigera, and T. P. Straatsma, "The missing term in effective pair potentials," *J. Phys. Chem.*, vol. 91, p. 6269, 1987.

[53]W. A. Steele, "The physical interaction of gases with crystalline solids: I. gas-solid energies and properties of isolated adsorbed atoms," *Surf. Sci.*, vol. 36, p. 317, 1973.

[54]M. M. Dubinin, G. U. Rakhmatkariev, and A. A. Isirikyan, "Differential heats of adsorption and adsorption isotherms of alcohols on silicalite," *Bull. Acad. Sci. USSR Div. Chem. Sci.*, vol. 38, pp. 1950–1953, 1989.

[55]Y. Oumi, A. Miyajima, and J. Miyamoto, *Studies in surface science and catalysis*, vol. 142. Amsterdam: Elsevier, 2002.

[56]J. Rouquerol, F. Rouquerol, K. Sing, P. LLewellyn, and G. Maurin, *Adsorption by Powders and Porous Solids. Principles , Methodology and Applications*. London, UK: Academic Press, 2nd ed., 2014.

[57]W. L. Jorgensen, "Optimized intermolecular potential functions for liquid alcohols," *J. Phys. Chem.*, vol. 90, pp. 1276–1284, 1986.

[58]O. Suárez-Iglesias, I. Medina, M. de los Ángeles Sanz, C. Pizarro, and J. L. Bueno, "Self-diffusion in molecular fluids and noble gases: Available data," *J. Chem. & Eng. Data*, vol. 60, pp. 2757–2817, sep 2015.

[59]R. Zangi, "Water confined to a slab geometry: a review of recent computer simulation studies," *J. Phys. Cond. Mat.*, vol. 16, pp. S0953–8984, 2004.

[60]J. Martí, C. Calero, and G. Franzese, "Structure and dynamics of water at carbon-based interfaces," *Entropy*, vol. 19, p. 135, 2017.

[61]R. Krishna and J. M. van Baten, "Hydrogen bonding effects in adsorption of water-alcohol mixtures in zeolites and the consequences for the characteristics of the maxwell-stefan diffusivities," *Langmuir*, vol. 26, pp. 10854–10867, 2010.